Applied Clay Science 114 (2015) 273–282

Contents lists available at ScienceDirect

Applied Clay Science

journal homepage: www.elsevier.com/locate/clay

Research paper

Hydrotalcite derived (Cu, Mn)–Mg–Al metal oxide systems doped with palladium as catalysts for low-temperature methanol incineration

Magdalena Jabłońska, Lucjan Chmielarz *, Agnieszka Węgrzyn, Kinga Góra-Marek, Zofia Piwowarska, Stefan Witkowski, Ewa Bidzińska, Piotr Kuśtrowski, Anna Wach, Dorota Majda

Faculty of Chemistry, Jagiellonian University, Ingardena 3, 30-060 Kraków, Poland

ARTICLE INFO

Article history:
Received 21 December 2014
Received in revised form 6 April 2015
Accepted 13 May 2015
Available online xxxx

Keywords:
Hydrotalcite-like materials
Mixed metal oxides
Catalysis
Total oxidation
Methanol

ABSTRACT

Hydrotalcite derived (Cu, Mn)–Mg–Al mixed metal oxides, synthesized by coprecipitation method, were found to be effective catalysts for methanol incineration. Copper and/or manganese oxides deposited on commercial γ-Al_2O_3 and MgO were used as the reference catalysts. Cu–Mg–Al–O mixed oxide system was found to be the most active catalysts in a series of the hydrotalcite originated metal oxides and supported samples. On the other hand, copper deposited on Al_2O_3 and MgO supports were significantly less active than the hydrotalcite derived catalysts. Activity of the catalysts was improved by deposition of small amount of palladium (0.5 wt.%). Temperature-programmed surface reaction method (CH_3OH-TPSR) and *in situ* Fourier-transform infrared spectroscopy (FT-IR) were employed to study the species formed on the catalyst surface during the process of methanol oxidation.

1. Introduction

Catalytic incineration of volatile organic compounds (VOCs) is one of the most promising ways to limit their emission into the atmosphere (Okumura et al., 2003). In contradiction to thermal oxidation of VOCs, the catalytic method operates at relatively lower temperatures and therefore undesired side processes, like the formation of NO_x by high temperature reaction of oxygen and nitrogen, are limited. Various types of materials were tested as potential catalysts for the total oxidation of VOCs. Catalytic systems containing Cu and Mn were found to be the most promising (e.g. Bahranowski et al., 1999; Gandia et al., 2002). Also the catalysts doped with noble metals (e.g. Pd) presented very interesting catalytic properties (e.g. Cordi and Falconer, 1996; Hosseini et al., 2009). At the same time, there is an increasing number of reports presenting the use of hydrotalcite-like materials as precursors of high surface area oxide catalysts. Such materials were found to be effective catalysts of various processes including also VOC incineration. An example could be successful use of the hydrotalcite derived Mg–Mn–(Al) mixed oxides in catalytic combustion of methane and toluene reported by Velu et al. (1999) and Jirátová et al. (2002). Otherwise, the hydrotalcite derived Co–Mn–Al oxide catalysts were reported to be active and selective for toluene (Lamonier et al., 2007) and ethanol (Kovanda et al., 2006) incineration. Lamonier et al. (2007) reported that the Mn-containing samples, especially hydrotalcite derived Co–Mn–Al mixed oxides with the molar ratio of Co:Mn:Al = 2.0:4.0:2.0, exhibited high activity in toluene oxidation. Cheng et al. (2008) showed that the Cu–Co–Mn–Al oxide catalyst (Cu:Co:Mn:Al = 1.0:2.0:0.2:0.8) was more active in methane combustion than the Cu–Co/X–Al (X = Fe, La, Ce) catalysts. The presence of the mixed phases containing both Mn and Co was suggested to influence the formation of structural defects, responsible for the improvement of oxygen mobility.

There are some reports related to the applications of the hydrotalcite derived Cu- (e.g. Kovanda et al., 2001; Chmielarz et al., 2012) and Cu–Mn-containing catalysts for VOC incineration (e.g. Zimowska et al., 2007; Cheng et al., 2008; Palacio et al., 2010; Aguilera et al., 2011; Kovanda and Jirátová, 2011a, 2011b; Ludvíková et al., 2012). For example, the catalytic behavior of Cu–Mn–Al (Cu:Mn:Al = 3.0:3.0:1.0) mixed metal oxide in total oxidation of toluene was studied by Palacio et al. (2010). The comparison of toluene incineration in the presence of calcined Cu–Mn–Al hydrotalcites (Cu:Mn:Al = 3.0:3.0:1.0 (Palacio et al., 2010) and (Cu:Mn:Al = 6.0:2.0:1.0 (Zimowska et al., 2007)), showed that the catalyst with smaller copper content was much more active. Temperature needed for 50% conversion of toluene to CO_2 (T_{50} = 258 °C) was among the lowest reported in literature presenting the application of hydrotalcite derivatives for the catalytic combustion of toluene (e.g. Kovanda et al., 2001; Lamonier et al., 2007; Mikulová et al., 2007; Zimowska et al., 2007). Similar activity in toluene oxidation was achieved for Cu–Mn–Mg–Al oxide system (T_{50} = 265 °C) (Aguilera et al., 2011).

The above reports were inspiration to the present studies, which are focused on determination of the role of manganese and copper in the process of methanol incineration, which was used as a model VOC molecule. Moreover, the present studies include analysis of the activating effect of palladium addition into the hydrotalcite based catalysts.

* Corresponding author. Tel.: +48 126632006; fax: +48 126340515.
E-mail address: chmielar@chemia.uj.edu.pl (L. Chmielarz).

http://dx.doi.org/10.1016/j.clay.2015.05.027
0169-1317/

Catalytic performance of the hydrotalcite originated catalysts was compared with the reference supported catalysts (Cu or/and Mn deposited on Al_2O_3, MgO, Mg–Al–O). Another goal of the present studies was the recognition of the reaction mechanism over the studied catalysts.

2. Experimental

2.1. Catalyst preparation

The Mg(II)–Al(III), Mn(II)–Mg(II)–Al(III), Cu(II)–Mg(II)–Al(III), Cu(II)–Mn(II)–Mg(II)–Al(III) hydrotalcite-like samples with the intended molar ratios of 71.0:29.0, 5.0:66.0:29.0, 5.0:66.0:29.0 (0.5:70.5:29.0) and 2.5:2.5:66.0:29.0, respectively, were synthesized by coprecipitation method using 1 M aqueous solutions of the following metal nitrates: $Cu(NO_3)_2 \cdot 3H_2O$ (Merck), $Mn(NO_3)_2 \cdot 4H_2O$ (Lach-Ner), $Mg(NO_3)_2 \cdot 6H_2O$ (Sigma) and $Al(NO_3)_3 \cdot 9H_2O$ (Fluka). A solution of NaOH (POCh) was used as the precipitating agent. Metal nitrate solutions were added to a vigorously stirred solution containing a slight over-stoichiometric excess of Na_2CO_3 (POCh). The pH was maintained at 9.0 ± 0.2 (with an exception of Cu(II)–Mg(II)–Al(III) synthesized at pH = 10.0 ± 0.2) by dropwise addition of 1 M NaOH solution. The obtained slurry was aged at 60 °C for 1 h, filtered, washed with distilled water and dried at room temperature (RT). For the Mn-containing hydrotalcite-like samples the syntheses were done under an argon atmosphere in order to avoid oxidation of Mn^{2+} cations.

The samples with the intended Cu or Mn content of 1 wt.% deposited on γ-Al_2O_3 (Merck) or MgO (POCh) by incipient wetness impregnation were used as the reference catalysts. In case of bimetallic catalysts (Cu–Mn or Mn–Cu, the sequence of metal deposition) intended total metals loading was 1 wt.%. The impregnated samples were calcined at 600 °C for 12 h.

The Pd-doped samples were prepared by incipient wetness impregnation of the samples with palladium standard for atomic absorption (1000 μg/cm^3, Witko) to obtain 0.5 wt.% of Pd loading. Then the samples were dried, calcined at 500 °C for 3 h and crushed (0.160–0.315 mm).

2.2. Catalyst characterization

The structure and crystallinity of the samples were analyzed by an X-ray powder D2 Phaser diffractometer (Brucker) using Cu Kα radiation (λ = 1.54060 Å, 30 kV, 10 mA). Cell parameters *a* and *c* were determined by analysis of (110) reflection and basal (003) and (006) reflections, respectively. Crystal sizes were calculated from the Scherrer equation.

Relative bulk chemical analysis of the calcined samples was done using Energy-Dispersive XRF spectrometer (Thermo Scientific, ARL QUANT'X). 150 mg of the powder sample was used to make a pellet. X-rays in the range of 4–50 kV (1 kV step) were generated by Rh anode. Detector used was 3.5 mm Si(Li) drifted crystal with Peltier cooling. For quantitative analysis, UniQuant software was used with a series of metallic standards.

The X-ray photoelectron spectra were recorded on a Prevac photoelectron spectrometer equipped with a hemispherical VG SCIENTA R3000 analyzer. The spectra were measured using a monochromatised aluminum AlKα source (E = 1486.6 eV) and a low energy electron flood gun (FS40A-PS) to compensate the charge on the surface of non-conductive samples. The base pressure in the analysis chamber during the measurements was 5×10^{-9} mbar. Spectra were recorded with constant pass energy of 100 eV. The binding energies were referenced to C 1s core level (E_b = 285.0 eV). The surface composition was determined on the basis of the areas and binding energies of Cu 2p, Mn 2p, Mg 2p, Al 2p, O 1s and C 1s photoelectron peaks. The fitting of high resolution spectra was provided through CasaXPS software.

Thermal decomposition of the hydrotalcite-like samples was studied by thermogravimetric method combined with on-line analysis of gaseous products (TG-DTA-QMS). The TG and DTA measurements of each sample (20 mg) were carried out using a Mettler Toledo 851^e thermobalance operated under a flow of air (80 cm^3/min) in the temperature range of 25–1000 °C with a linear heating rate of 10 °C/min. The gases evolved during the thermal decomposition of the samples were continuously monitored with a quadruple mass spectrometer (QMS) ThermoStar (Balzers) connected directly to the thermobalance.

The specific surface area (S_{BET}) of the samples was determined by low-temperature (−196 °C) N_2 sorption using Quantasorb Junior sorptometer (Ankersmit). Prior to nitrogen adsorption the samples were outgassed in a flow of nitrogen at 250 °C for 2 h.

The state of transition metals and the chemical environment were recorded at −196 °C using an ELEXSYS E-500 (Bruker) spectrometer operating at 100 kHz field modulation. Prior to EPR measurements the samples were outgassed under high vacuum.

The type of transition metal species and their aggregation were analyzed by UV–vis-DR spectroscopy using an Evolution 600 (Thermo) spectrometer. The spectra were recorded at RT in the range of 200–900 nm with a resolution of 1 nm.

The redox properties of the catalysts were studied by temperature-programmed reduction (H_2-TPR). The experiments of each samples (30 mg) were performed in a fixed-bed flow microreactor system starting from RT to 1100 °C, with a linear heating rate of 5 °C/min. H_2-TPR runs were carried out in a flow (6 cm^3/min) of 5 vol.% H_2 diluted in Ar. Water vapor was removed from effluent gas by the means of a cold trap. The consumption of hydrogen was monitored by micro volume TCD detector (Valco).

2.3. Catalytic studies

The obtained samples were tested as catalysts of methanol incineration. The catalytic experiments were performed under atmospheric pressure in a fixed-bed flow microreactor system. The reactant concentrations were continuously measured using a quadruple mass spectrometer (QMS) RGA 200 (PREVAC) connected directly to the reactor outlet. Prior to the catalytic test each catalyst sample (100 mg) was outgassed in a flow of air at 400 °C for 30 min. An isothermal saturator with a constant flow of air was used for supplying of methanol into the reaction mixture. The composition of gas mixture at the reactor inlet was [CH_3OH] = 4.0 vol.%, [O_2] = 19.0 vol.% and [N_2] = 77.0 vol.%. Total flow rate of the reaction mixture was 20 cm^3/min. The reaction was studied in the range of 150–400 °C with a linear temperature increase of 10 °C/min.

2.4. Studies on the reaction mechanism

The interaction of the catalysts with methanol at different temperatures was studied by temperature-programmed surface reaction (CH_3OH-TPSR) and *in situ* FT-IR.

The CH_3OH-TPSR measurements were performed in a fixed-bed flow microreactor system equipped with a QMS detector—RGA 200 (PREVAC). Prior to methanol sorption the sample (100 mg) was outgassed in a flow of air at 550 °C (800 °C for the MgO-based samples) for 30 min. Subsequently, the microreactor was cooled down to 70 °C and the sample was saturated in a flow (20 cm^3/min) of gas mixture containing 4 vol.% of methanol diluted in helium for about 3.5 h. Then, the sample was purged in a flow of pure helium (about 1.5 h). In the next step reactor temperature was raised in the range of 70–550 °C (70–800 °C for the MgO-based samples) in a flow of air (20 cm^3/min).

Transformation of methanol over the catalysts was followed also by FT-IR spectroscopy (Equinox 55 Bruker spectrometer equipped with a MCT detector). A self-sustaining pellet of the sample was degassed at 480 °C for 1 h under high vacuum and then cooled to RT. The catalyst was contacted with methanol vapor (1333 Pa in the gas phase) at RT, then IR cell was heated up to 300 °C and kept at this temperature for 5 min. After that time IR cell cooled down to all product of methanol

oxidation could be detected. All the spectra were recorded at RT and, then, normalized to 10 mg of the sample.

3. Results and discussion

Examples of powder XRD diffraction patterns, recorded for the Ht–Mg–Al and Ht–Cu–Mn–Mg–Al hydrotalcite-like materials and their calcined forms, are presented in Fig. 1A. The obtained precursors exhibit a typical crystalline hydrotalcite-like structure belonging to the space group R3m in the trigonal symmetry (Węgrzyn et al., 2010). It should be mentioned that for all the as-synthetized samples very similar XRD patterns were recorded. Cell parameters and crystallite sizes of the hydrotalcite-like samples, determined from XRD measurements, are presented in Table 1. The cell parameter *c* for hydrotalcite-like materials is about 2.3 nm, which is typical of hydrotalcites containing carbonates as interlayer anions (Chmielarz et al., 2011). XRD patterns of the calcined samples contain only reflections typical of poorly crystallized MgO-type mixed oxides (reflections at 36°, 43° and 63°) belonging to the space group Fm3m (Millange et al., 2000). Similar XRD patterns were recorded also for Cu–Mg–Al and Mn–Mg–Al (results not shown). For the samples doped with 0.5 wt.% of Pd no evidence of the segregated phases corresponding to palladium or its oxide (PdO) was found. It could be explained by high and stable dispersion of deposited palladium. It should be noted that in diffractograms of the samples doped with palladium sharp peaks corresponding to a highly crystallized MgO were found (Fig. 1B). Similar phenomenon was reported for platinum impregnated MgO by Aramendía et al. (1999), who showed that the sample obtained using an aqueous solution of H_2PtCl_6 was more crystalline than its counterpart prepared from nitrate salt. Moreover, it was suggested that the simultaneous presence of both noble metal and chloride is crucial for the complete reconstruction of the primary structure and consequently the formation of highly crystalline MgO. Our studies show that similar effect is possible in the presence of palladium and chloride. However, detailed explanation of this interesting effect needs separate studies.

Table 1
Structural parameters of hydrotalcite-like precursors.

Sample code	FWHM of (003)	Cell parameter	Crystallite size	Cell parameter	Crystallite size
	Peak [2Θ]	*a* [nm]	*Da* [nm]	*c* [nm]	*Dc* [nm]
Ht–Mg–Al	1.1106	0.3046	24	2.2888	15
Ht–Cu–Mg–Al	1.1142	0.3050	26	2.2868	15
Ht–Cu–Mn–Mg–Al	1.6237	0.3054	26	2.3155	13
Ht–Mn–Mg–Al	1.3920	0.3062	29	2.3121	15

Thermal decomposition of hydrotalcite-like materials was studied by thermogravimetric analysis coupled with the analysis of gaseous products by QMS detector. The *m/z* signals obtained were 18—H_2O, 44—CO_2, 30—NO (and possibly also NO_2) and 46—NO_2. Fig. 2 presents the weight loss of the hydrotalcite-like samples with various cationic compositions during heating in a flow of air, revealing the transformation into corresponding mixed metal oxides.

For Mg–Al hydrotalcite an endothermic process related to the removal of interlayer and weakly adsorbed water took place up to 250 °C. The unresolved double DTG minima centered at 344 and 381 °C are a result of water vapor evolution formed as a product of dehydroxylation of OH^- anions of the brucite-like layers. The evolution of CO_2 and very small amounts of NO (possibly also NO_2) is related to thermal decomposition of interlayer anions CO_3^{2-} and NO_3^-, respectively. However, it cannot be excluded that evolution NO (possibly also NO_2) is a result of residual nitrates decomposition in salts remaining after washing of the hydrotalcite sample. It should be noted that small amounts of carbonates were stable at temperatures as high as 600 °C.

A partial replacement of Mg cations by Cu ions in the brucite-like layers resulted in modification of the DTG curve shape. In this case,

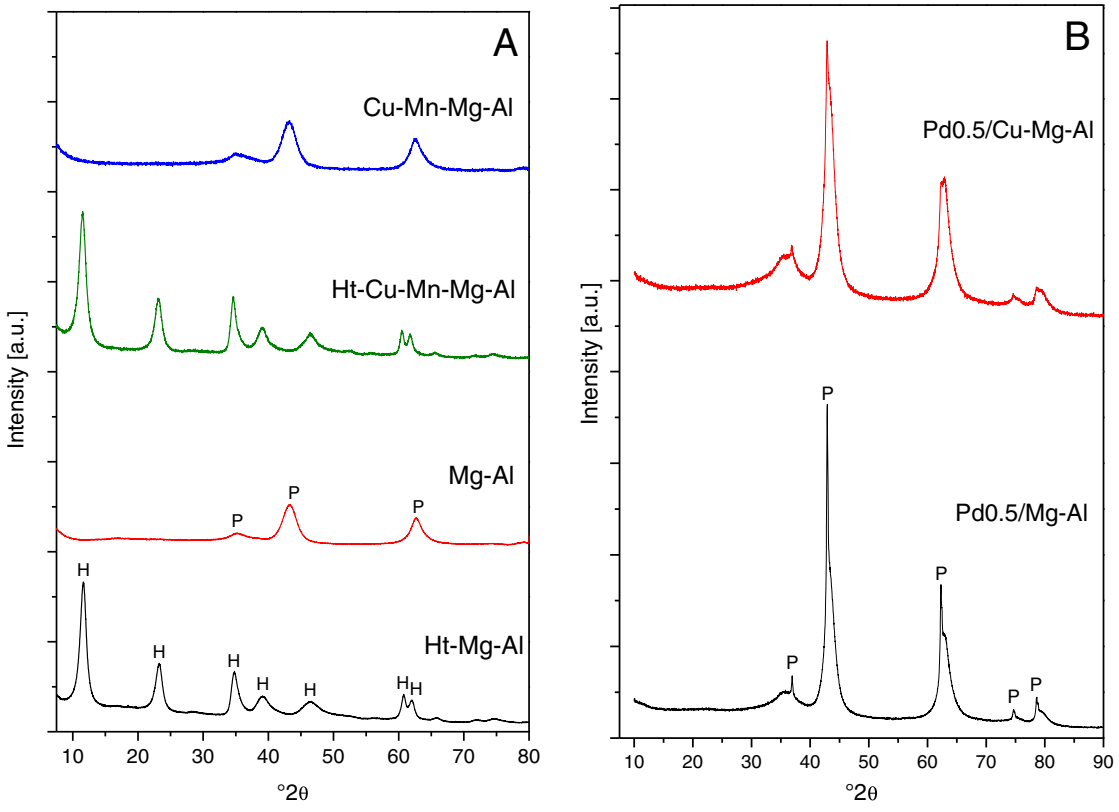

Fig. 1. Examples of X-ray diffraction patterns of hydrotalcite-like precursors: Ht–Mg–Al, Ht–Cu–Mn–Mg–Al and their calcined forms Mg–Al, Cu–Mn–Mg–Al (A), and Pd-impregnated and calcined materials (B); H—hydrotalcite-like materials, P—periclase (MgO).

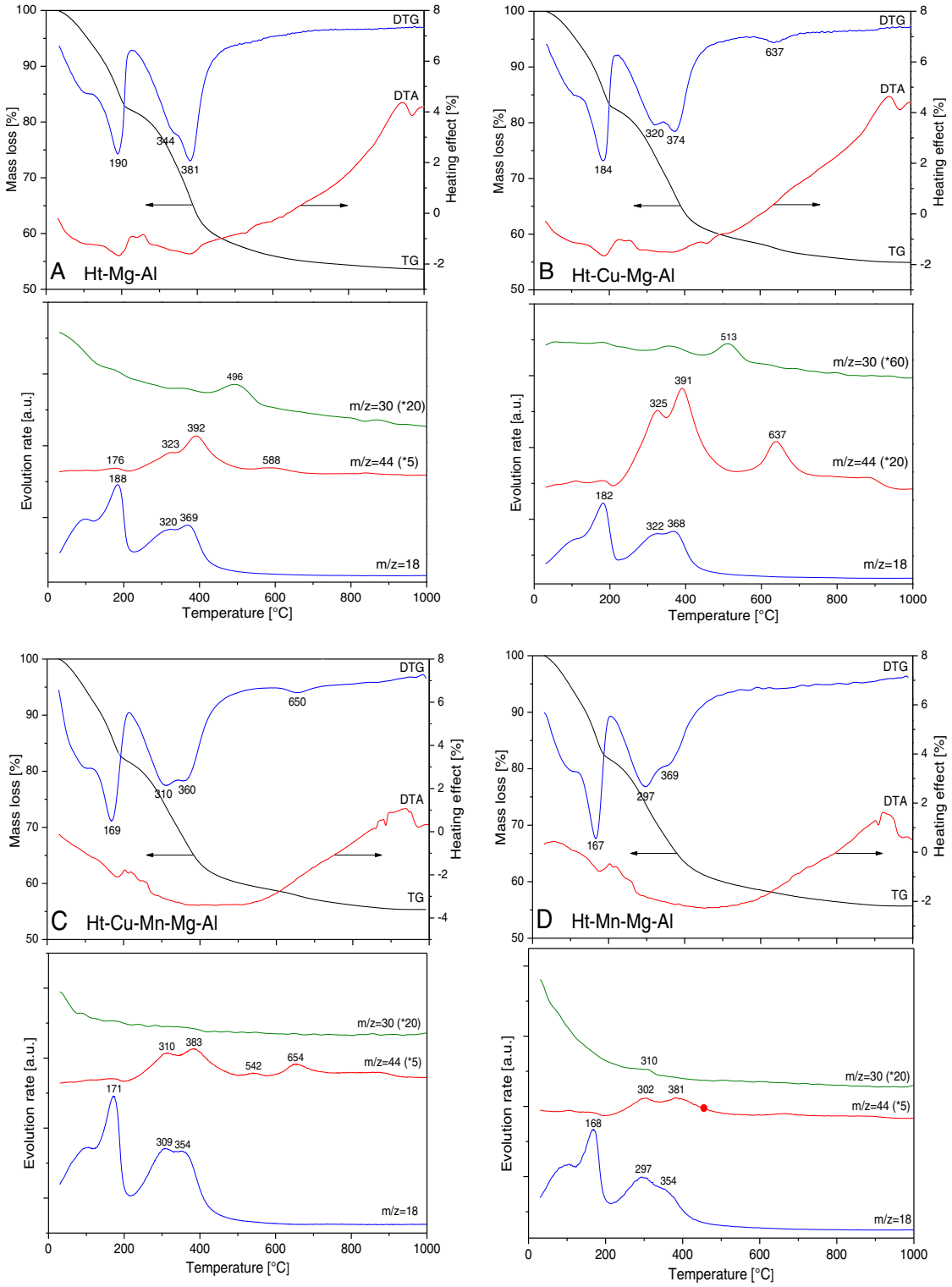

Fig. 2. Results of TGA-DTA with analysis of m/z signals of 18 (H_2O), 44 (CO_2) and 30 (NO and possibly also NO_2) by QMS during thermal decomposition of hydrotalcite-like materials: Ht–Mg–Al (A), Ht–Cu–Mg–Al (B), Ht–Cu–Mn–Mg–Al (C), Ht–Mn–Mg–Al (D). Experimental conditions: mass of sample = 20 mg, flow of synthetic air = 80 cm^3/min, liner heating rate of 10 °C/min.

decomposition processes occurred at lower temperatures. This phenomenon can be explained by partial distortion of the hydrotalcite structure due to incorporation of Cu cations into Mg–Al brucite-like sheets (Jahn–Teller effect) as it was earlier suggested (e.g. Bastiani et al., 2004). The removal of interlayer and weakly adsorbed water from the Cu–Mg–Al hydrotalcite-like sample was manifested by a peak centered at 184 °C. Two DTG peaks at 320 and 374 °C can be ascribed to dehydroxylation of the brucite-like layers and thermal decomposition of interlayer carbonate anions. The presence of high temperature peak of CO_2 evolution centered at 637 °C is related to decomposition of thermally stable CO_3^{2-} anions. Possibly, copper was responsible for the stabilization of such carbonate anions.

Incorporation of manganese into the brucite-like layers, led to a further decrease in temperature of their decomposition. This effect could

be explained by a decrease in crystallinity of Mn-containing hydrotalcite-like materials. This hypothesis is supported by XRD results, wherein the FWHM value increased after incorporation Mn into the Cu–Mg–Al and Mg–Al hydrotalcite-like structure (see Table 1). Similar results were reported earlier by Velu et al. (1999) and interpreted as distortion of the hydrotalcite-like structure induced by substitution of manganese into the Mg–Al hydrotalcite-like framework.

The specific surface area (S_{BET}) of the calcined samples and their modifications with palladium are shown in Table 2. S_{BET} of the samples depends on their chemical composition. It should be noted that incorporation of copper and/or manganese into the hydrotalcite-like framework, reduces their surface area compared to the calcined Mg–Al sample. Deposition of palladium onto the calcined samples resulted in a further decrease of their specific surface area.

The oxidation states and chemical environment of Cu and/or Mn species present in hydrotalcite-like materials and their calcined forms were studied by EPR method. Fig. 3 presents the X-band EPR spectra of the as-prepared (Ht–Cu–Mg–Al, Ht–Cu–Mn–Mg–Al, Ht–Mn–Mg–Al) and calcined (Cu–Mn–Mg–Al, Mn–Mg–Al) hydrotalcite-like samples. The EPR spectrum of Ht–Cu–Mg–Al exhibits a broad, unstructured and slightly axial signal with a partial resolution in the parallel region only. Cu^{2+} is present in the form of mononuclear and clustered species (Centi et al., 1995). Any evidence of the hyperfine structure in the EPR spectra of this sample is a result of copper ions interacting, which are sufficiently close to one another (Centi et al., 1995). The EPR spectrum obtained for the Ht–Cu–Mn–Mg–Al sample, shows four hyperfine lines centered around $g = 2.064$ with an average hyperfine coupling constant A of 87 G, indicating the existence of Mn^{2+} ions in a distorted octahedral coordination in the brucite-like layer. Similar EPR results were reported by Velu et al. (1999) for Mn–Mg–Al hydrotalcite-like materials and by Xu et al. (1998) for Mn-MCM-41 or by Levi et al. (1991) for MnAPOs with Mn present in the extra-framework positions.

As the manganese content in the Ht–Mn–Mg–Al sample increased, the EPR spectrum exhibits only a single line with $g = 1.993$ and Lorentzian shape corresponding to Mn^{2+} species. The hyperfine line was not observed in this spectrum, indicating strong spin–spin interactions, i.e. the magnetic dipole interaction and exchange interaction for that manganese content (Brouet et al., 1992). Part of manganese retained its +2 oxidation state even upon calcination in air at 600 °C due to the formation of Mn_3O_4 ($MnO–Mn_2O_3$) spinel. Mn^{2+} cations in the Mn–Mg–Al sample showed g value of 2.043. It should be noted that signal related to the presence of Mn^{2+} cations was drastically reduced, what is related to the oxidation of majority of these cations during calcination process. For the Cu–Mn–Mg–Al sample a superposition of the EPR spectra of the one-component systems was observed, which indicates the formation of the separate Cu- and Mn-containing phases.

Table 2
BET surface area of the catalytic materials.

Sample codes	BET area [m^2/g]
Mg–Al	173
Mn–Mg–Al	161
Cu(5)–Mg–Al[a]	121
Cu (0.5)–Mg–Al[b]	168
Cu–Mn–Mg–Al	158
Pd0.5/Mg–Al	130
Pd0.5/Mn–Mg–Al	120
Pd0.5/Cu(5)–Mg–Al[a]	84
Pd0.5/Cu–Mn–Mg–Al	103
Al_2O_3	135
Mn/Al_2O_3	99
Cu/Al_2O_3	98
$Cu–Mn/Al_2O_3$	100
$Mn–Cu/Al_2O_3$	101
MgO	40
Mn/MgO	38
Cu/MgO	29
Cu–Mn/MgO	27
Mn–Cu/MgO	34

[a] The samples obtained from hydrotalcite-like precursor with the intended Cu(II)–Mg(II)–Al(III) molar ratio of 5.0:66.0:29.0.
[b] The samples obtained from hydrotalcite-like precursor with the intended Cu(II)–Mg(II)–Al(III) molar ratio of 0.5:70.5:29.0.

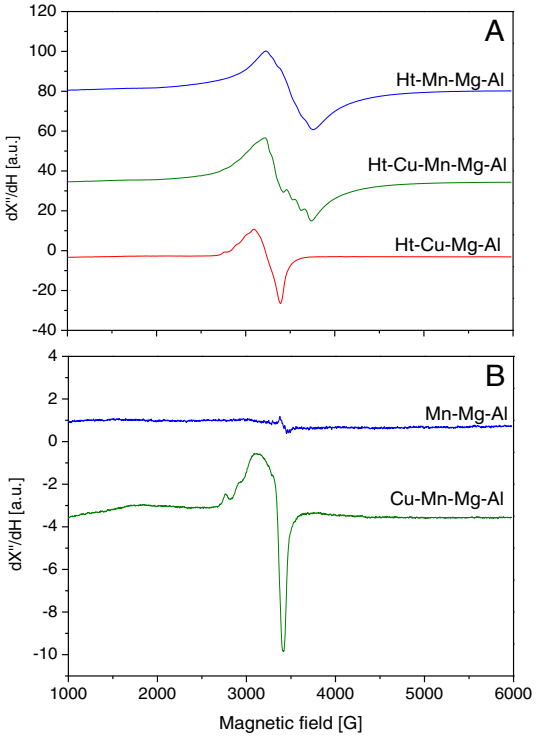

Fig. 3. EPR spectra of hydrotalcite-like materials: Ht–Cu–Mg–Al, Ht–Cu–Mn–Mg–Al, Ht–Mn–Mg–Al (A), calcined materials: Cu–Mn–Mg–Al, Mn–Mg–Al (B).

The UV–vis-DRS was employed to determine coordination and aggregation of transition metals present in the samples. Fig. 4 presents the UV–vis DR spectra of the Ht–Cu–Mg–Al, Ht–Cu–Mn–Mg–Al, Ht–Mn–Mg–Al hydrotalcite-like samples and their calcined forms. The literature data related to the absorption bands of charge-transfer and d–d transition in copper, manganese and/or palladium in different chemical environment are presented in Table 3.

The diffuse reflectance spectrum of the as-prepared Ht–Cu–Mg–Al sample exhibits strong absorption at around 220 nm and broad band around 700 nm. As it can be seen from Table 3, these bands are attributed to charge-transfer between mononuclear Cu^{2+} ion and oxygen and d–d transition in Cu^{2+} ions in octahedral environment. Similar bands at about 226 and 700 nm are present in the Ht–Cu–Mn–Mg–Al sample. Moreover, a broad band at about 400 nm assigned to the $O^{2-} \rightarrow Mn^{3+}$ charge transfer transition was found for the Ht–Mn–Mg–Al and Ht–Cu–Mn–Mg–Al samples. The bands located at 210 and 250 nm in a spectrum of the Ht–Mn–Mg–Al sample can be attributed to the allowed $O^{2-} \rightarrow Mn^{2+}$ charge transfer transition.

The UV–vis DR spectrum of the calcined Cu(5)–Mg–Al sample consists of the band located around 265 nm with a shoulder at about 350 nm and a broad band above 700 nm. These bands are related charge-transfer between mononuclear Cu^{2+} ion, charge-transfer between Cu^{2+} and oxygen in oligonuclear $[Cu–O–Cu]_n$ species and d–d transition in Cu^{2+} ions in octahedral environment, respectively (see Table 3).

For the Mn–Mg–Al samples the UV–vis-DR spectrum consists of main absorption broad band located below 400 nm, which is a superposition of bands related to charge-transfers transition of $O^{2-} \rightarrow Mn^{2+}$ and $O^{2-} \rightarrow Mn^{3+}$ in Mn_3O_4 spinel as well as $^5B_{1g} \rightarrow {}^5B_{2g}$ transition related to Mn^{3+} in Mn_2O_3. The shoulder at about 485 nm is assigned to the $^5B_{1g} \rightarrow {}^5E_g$ crystal field d–d transitions in Mn_2O_3 or alternatively to

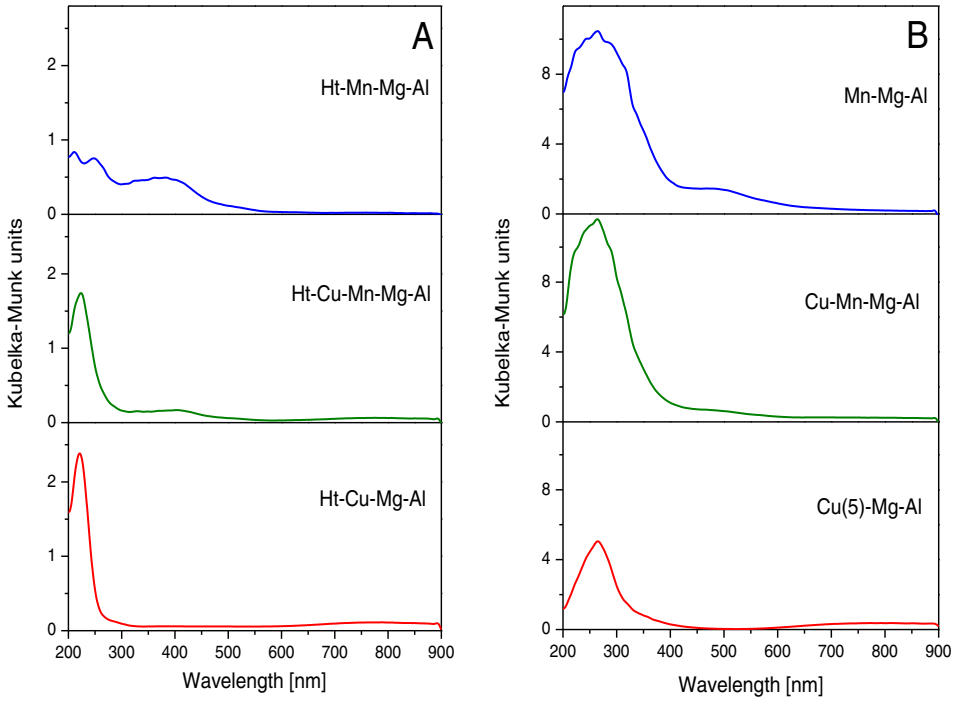

Fig. 4. UV–vis DR spectra of the hydrotalcite-like precursors: Ht–Cu–Mg–Al, Ht–Cu–Mn–Mg–Al, Ht–Mn–Mg–Al (A), calcined materials: Cu(5)–Mg–Al, Cu–Mn–Mg–Al, Mn–Mg–Al (B).

$^4A_{2g} \rightarrow {}^4T_{2g}$ crystal field transition in Mn^{4+} (see Table 3). Deposition of small amounts of palladium on calcined hydrotalcite-like materials does not generate any new bands but intensity of the bands characteristic of Cu- and Mn-species increased and were shifted to higher wavelength. Probably this effect was caused by the phase segregation that occurred after the second calcination at 500 °C.

Fig. 5 presents the H_2-TPR profiles obtained for the calcined Cu(5)–Mg–Al, Cu–Mn–Mg–Al, Mn–Mg–Al samples and their modifications with palladium. The TPR profile of Cu(5)–Mg–Al consists of a sharp peak at 300 °C and a broad reduction peak above 450 °C. According to Chmielarz et al. (2003) the low-temperature peak can be attributed to the reduction of Cu^{2+} cations in CuO to metallic copper, while the broad peak above 450 °C to hydrogenation of residual carbonates. The TPR profile obtained for Mn–Mg–Al consists of two very broad peaks centered at about 280 and 520 °C. The high-temperature peak could be attributed to the reduction of Mn_2O_3 to Mn_3O_4 spinel (e.g. Tang et al., 2010), while low-temperature shoulder to the reduction of dispersed MnO_x species (e.g. Stobbe et al., 1999). The H_2-TPR profile obtained for Cu–Mn–Mg–Al contains an intensive peak at about 322 °C, attributed to the reduction of CuO to Cu^0, and broad maximum at about 580 °C attributed to the hydrogenation of residual carbonates. No peaks attributed to the reduction of MnO_x were observed, although coexistence two reducible phases in the sample (CuO, MnO_x) may be assumed. A similar result was reported by Kovanda et al. (2005). It should be noted that the reduction peak of Cu–Mn–Mg–Al was shifted to higher temperatures comparing to Cu(5)–Mg–Al counterpart, indicating that MnO_x retarded the CuO reduction (Li et al., 2006).

Introduction of palladium into the catalysts shifted the reduction peaks to lower temperatures. This effect could be explained by hydrogen dissociation and spill-over on noble metal during H_2-TPR runs (e.g. Gauthard et al., 2003). For Pd0.5/Cu(5)–Mg–Al and Pd0.5/Cu–Mn–Mg–Al, the reduction profiles were spitted into two peaks centred at about 245, 280 °C and at about 230, 305 °C, respectively. This effect could be explain by parallel reduction of CuO by molecular H_2 (higher temperature) or by hydrogen species dissociated on palladium (lower temperature). It should be also noted that there are not peaks attributed to the reduction of palladium oxide in TPR profiles. It could be explained

Table 3
The literature data related to charge-transfer and d–d transfer transitions of Cu, Mn and Pd reference compounds.

Compound	M^{n+}	λ_{max} [nm]	Assignment	Reference
CuO	Cu^{2+}	240	$O^{2-} \rightarrow Cu^{2+}$	Crivello et al. (2005)
		700	$^2E_g \rightarrow {}^2T_{2g}$	Marion et al. (1990)
$[Cu–O–Cu]_n$	Cu^{2+}	350	$O^{2-} \rightarrow Cu^{2+}$	Mendes and Schmal (1997)
Mn_3O_4	Mn^{2+}	255	$O^{2-} \rightarrow Mn^{2+}$	Baldi et al. (1998)
	Mn^{3+}	320	$O^{2-} \rightarrow Mn^{3+}$	
Mn_2O_3	Mn^{3+}	370	$^5B_{1g} \rightarrow {}^5B_{2g}$	Baldi et al. (1998)
		485	$^5B_{1g} \rightarrow {}^4E_g$	
$Mn–Al_2O_3$	Mn^{4+}	470	$^4A_{2g} \rightarrow {}^4T_{2g}$	Kijlstra et al. (1997)
PdO	Pd^{2+}	204	$Pd^{2+} \rightarrow Pd^{2+}$	Ivanova et al. (2010)
		332	$Pd^{2+} \rightarrow O^{2-}$	Gaspar and Dieguez (2000)
		400	$^3A_{2g} \rightarrow {}^3T_{2g}$	Ivanova et al. (2010)

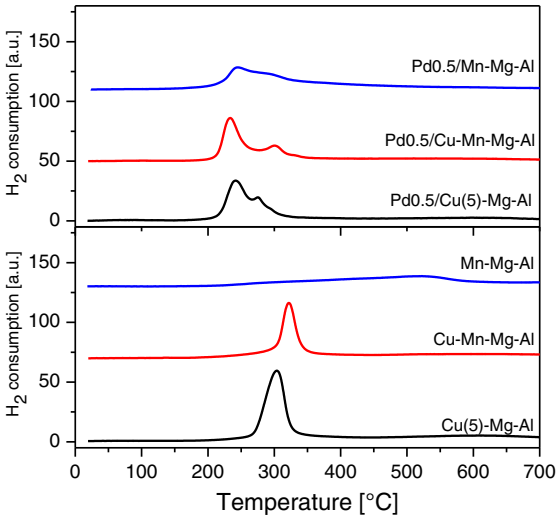

Fig. 5. Results of H_2-TPR studies of the hydrotalcite originated catalysts and their modifications with palladium: mass of catalyst = 30 mg, flow (6 cm^3/min) of 5 vol.% H_2 diluted in Ar, linear temperature increase of 5 °C/min.

by too low amount of palladium introduced into the studied catalysts (Carnö et al., 1997).

Because of doubts related to the oxidation states of manganese in the Mn–Mg–Al sample, the XPS spectrum of Mn 2p core level was recorded (Fig. 6). Two peaks corresponding to the Mn $2p_{1/2}$ and Mn $2p_{3/2}$ components are found at 653.8 eV and 642.3 eV, respectively. The 11.5 eV difference between these two states is owing to the spin–orbital splitting. Furthermore, multiplet splitting results in asymmetry of the measured lines. The value of binding energy for the Mn $2p_{3/2}$ line and its shape suggests the presence of mainly Mn^{3+} species on the catalyst surface. The difference between the binding energies of the Mn $2p_{3/2}$ and O 1s levels equal to 112.2 eV also confirms such assumption (Kosova et al., 1999). Unfortunately, using the Mn 3s peak to distinguish Mn oxidation state is unhelpful due to its low intensity and the overlapping Mg 2s line.

Taking into account the results of XPS, UV–vis-DRS, EPR and H_2-TPR studies focused on determination of Mn oxidation states in the calcined hydrotalcite originated samples it could be suggested that manganese is present mainly in the form of Mn^{3+} with a small contribution of Mn^{2+} (possibly in Mn_3O_4 spinel) in the core of catalyst grains. On the other hand copper in the form of Cu^{2+} ions was identified in the samples.

The chemical composition of the copper containing samples, determined by XRF method, was compared with the surface composition of these catalysts, determined by XPS method in Table 4. It should be noted that in case of all the analyzed samples their surface is significantly enriched with copper comparing to the bulk content of this transition metal. Of course, this effect is more significant for the reference supported catalysts. Thus, there is a different surface contribution of copper species available for the catalytic process in the studies samples.

Calcined hydrotalcite-like materials and their modifications with palladium were tested as catalysts for methanol incineration. CO_2 and water vapour were the only detected reaction products. The activity of the catalysts is frequently characterized by two parameters, T_{50} and T_{90}, which for the studied catalysts are summarized in Table 5. T_{50} refers to temperature needed to reach 50% methanol conversion, and is used to compare catalytic activity in the same reaction conditions, while T_{90} is temperature needed to obtain 90% methanol conversion. For all tested catalysts T_{50} was below 350 °C.

As it can be seen from Fig. 7 oxidation of methanol in a series of the hydrotalcite derived catalysts is the most efficient in the presence of Cu(5)–Mg–Al. In this case the reaction stared at about 225 °C, while the complete methanol oxidation was achieved at 325 °C. Although, the Mn-containing catalysts were reported in scientific literature to be quite active in the process of VOC combustion (e.g. Dula et al., 2007),

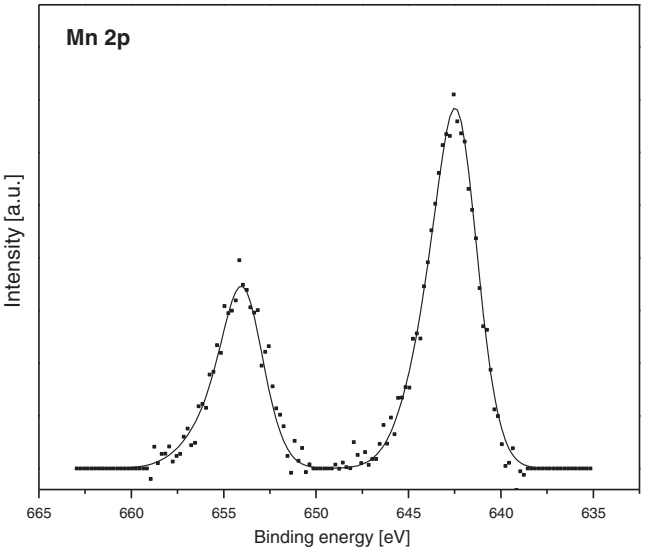

Fig. 6. XPS spectrum of Mn 2p core level for the Mn–Mg–Al catalyst.

Table 4
Total (XRF) and surface (XPS) chemical composition of the Cu-containing catalysts.

Sample codes	Total metal content [mol.%]			Surface metal content [mol.%]		
	Cu	Mg	Al	Cu	Mg	Al
Cu(5)–Mg–Al	3.96	60.63	35.41	6.86	61.10	32.04
Cu (0.5)–Mg–Al	0.40	63.33	36.27	0.70	64.67	34.63
Cu/Al_2O_3	0.58	0.00	99.42	1.82	0.00	98.18
Cu/MgO	0.76	99.24	0.00	2.28	97.72	0.00

the Mn-containing hydrotalcite-based catalyst was found to be significantly less active comparing to Cu(5)–Mg–Al. The catalyst containing both Cu and Mn (Cu–Mn–Mg–Al) presented intermediate activity between the Cu(5)–Mg–Al and Mn–Mg–Al catalysts at temperature above 260 °C. Introduction of palladium (0.5 wt.%) into the Cu(5)–Mg–Al, Cu–Mn–Mg–Al and Mn–Mg–Al catalysts resulted in a shift of the methanol conversion profile in direction of lower temperature for all tested catalysts. It can be clearly seen that the Cu-based catalysts doped with palladium (Pd0.5/Cu(5)–Mg–Al and Pd0.5/Cu–Mg–Mn–Al) are the most active in the studied reaction, while the Pd0.5/Mn–Mg–Al and Pd0.5/Mg–Al catalysts presented lower activity. Thus, the presence of copper is a key factor determining activity of the catalysts in methanol incineration, which can be additionally increased by incorporation of small amounts of palladium.

Fig. 7 presents also the results obtained for the reference catalysts based on transition metals (Cu or Mn) deposited on commercial supports (MgO and Al_2O_3) by impregnation method. It should be noted that the content of transition metals deposited on the supports is significantly lower in comparison to the most active Cu(5)–Mg–Al catalyst (c.f. Table 4). Therefore, the hydrotalcite based sample with significantly lower copper content (Cu(0.5)–Mg–Al), comparable to the studied supported Cu/Al_2O_3 and Cu/MgO catalysts, was prepared and tested in methanol incineration. As can be seen from Table 5 and Fig. 7, catalytic activity of this sample is significantly lower than Cu(5)–Mg–Al but also higher than Cu/Al_2O_3 and Cu/MgO. Thus, it could be concluded that copper in Mg–Al oxide matrix is more catalytically active in methanol incineration in comparison to copper deposited on the MgO or Al_2O_3 supports. Especially, taking into account the contribution of surface copper species available for the catalytic process on the surface of Cu(0.5)–Mg–Al and the supported reference samples presented in Table 4.

Table 5
T_{50} and T_{90} temperatures of methanol decomposition over (Cu, Mn)–Mg–Al catalysts.

Samples	T_{50} [°C]	T_{90} [°C]
Mg–Al	346	396
Mn–Mg–Al	302	340
Cu(0.5)–Mg–Al[a]	291	323
Cu(5)–Mg–Al[b]	252	275
Cu/Mg–Al	321	366
Cu–Mn–Mg–Al	285	319
Pd0.5/Mg–Al	216	247
Pd0.5/Mn–Mg–Al	222	250
Pd0.5/Cu(5)–Mg–Al[b]	191	220
Pd0.5/Cu–Mn–Mg–Al	195	228
Al_2O_3	295	431
Mn/Al_2O_3	314	347
Cu/Al_2O_3	289	347
$Cu–Mn/Al_2O_3$	296	330
$Mn–Cu/Al_2O_3$	277	321
MgO	324	372
Mn/MgO	276	319
Cu/MgO	307	356
Cu–Mn/MgO	321	367
Mn–Cu/MgO	259	320

[a] The samples obtained from hydrotalcite-like precursor with the intended Cu(II)–Mg(II)–Al(III) molar ratio of 0.5:70.5:29.0.
[b] The samples obtained from hydrotalcite-like precursor with the intended Cu(II)–Mg(II)–Al(III) molar ratio of 5.0:66.0:29.0.

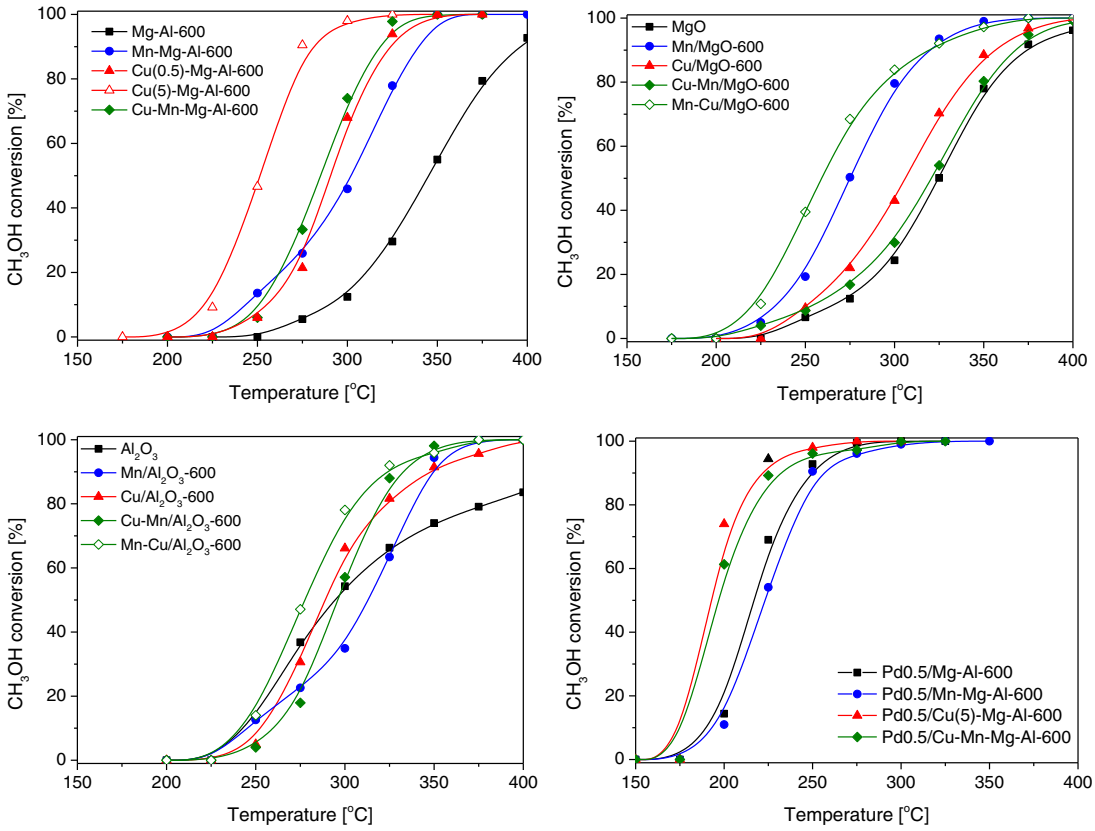

Fig. 7. Total oxidation of methanol performed in the presence of calcined and impregnated hydrotalcite-like materials and Al_2O_3 and MgO catalytic materials. Reaction conditions: mass of catalyst = 100 mg, [CH_3OH] = 4.0 vol.%, [O_2] = 19.0 vol.% and [N_2] = 77.0 vol.%, total flow rate = 20 cm^3/min, linear heating of 10 °C/min.

Interesting results of the catalytic tests were obtained by the sequential deposition of both Mn and Cu on MgO or Al_2O_3. First of all it should be noted that the sequence of metal depositions is very important to obtain active catalysts for methanol incineration. The more active catalysts were obtained by deposition of manganese (first step) followed by deposition of copper (second step) than for the reverse deposition order. It could be explained by higher activity of copper in comparison to manganese and therefore in case of the catalysts obtained by deposition of copper in a second step this metal was more exposed on the sample surface and more available for reactants. This hypothesis is supported by XPS studies performed for Cu–Mn/Al_2O_3, which showed that about 0.72 mol.% of Cu was exposed on the Al_2O_3 surface, while after deposition of manganese in the second step, the content of exposed copper was limited to about 0.55 mol.%.

The mechanism of the methanol incineration process over the hydrotalcite derived and reference supported catalysts was studied by the temperature-programed surface reaction and FT-IR methods. Fig. 8 presents the profiles of CO_2 evolution formed by the temperature-programed reaction of adsorbed methanol with oxygen (CH_3OH-TPSR). For the Cu(5)–Mg–Al catalyst significant amounts of adsorbed methanol were oxidized to CO_2, which was emitted at 240 °C. It should be noted that evolution of CO_2 was not observed at temperature above

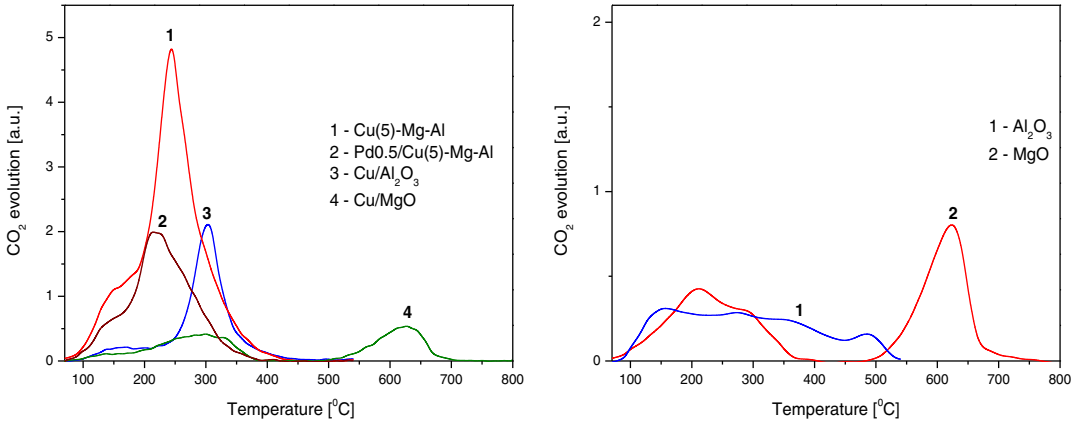

Fig. 8. Temperature-programmed surface reaction (CH_3OH-TPSR) performed for the selected catalysts as well as Al_2O_3 and MgO. Reaction conditions: mass of catalyst = 100 mg, adsorption of methanol at 70 °C in a flow of 4 vol.% CH_3OH diluted in helium, temperature-programmed surface reaction—flow of air = 20 cm^3/min, linear heating of 10 °C/min.

450 °C for these samples. Thus, it could be concluded that copper dispersed in the structure of calcined hydrotalcite plays an important role in the low-temperature oxidation of methanol and there is not strong interaction of CO_2 with the surface of this catalyst. Deposition of palladium on Cu (5)–Mg–Al shifted the peak of CO_2 evolution into temperature lower by about 25 °C and decreased its intensity. It is in agreement with the results of the catalytic tests (cf. Fig. 7). Evolution of CO_2 from the surface of the supported Cu/Al_2O_3 catalyst occurred at about 310 °C, what may suggest lower activity of copper species deposited on alumina comparing to the copper containing hydrotalcite based catalysts. Moreover, the comparison of the CO_2 evolution profiles obtained for Cu/Al_2O_3 and for Al_2O_3 shows that a peak at 310 °C is related to the presence of copper in the Cu/Al_2O_3 catalyst. The evolution of CO_2 from Cu/MgO occurred in two stages. Small amounts of CO_2 were produced at low temperature (below 400 °C). Moreover, the evolution of CO_2 was detected in the temperature range of 500–700 °C. The low-temperature peak could be related to direct evolution of CO_2 formed by oxidation of adsorbed methanol, while the high-temperature peak is possibly a result of the partial CO_2 capture in the form of carbonates deposited on the basic MgO surface (Hassanzadeh and Abbasian, 2010). Similar results were obtained for pure MgO, thus it seems that copper deposited on this support only slightly influences its surface properties towards CO_2 adsorption.

Information on the ability of methanol transformation over two selected samples Cu/MgO and Cu(5)–Mg–Al was provided from IR spectroscopic investigations. An excess of methanol (1333 Pa in the gas phase) was introduced over the Cu/MgO and Cu(5)–Mg–Al catalysts at RT. The presence of methanol, both adsorbed and in the gas phase, can be easily recognized in IR spectra (Fig. 9A, spectra a) as the 1480–1450 cm^{-1} set of bands of the CH_3– group vibrations. After 5 min contact time at 300 °C the IR cell was cooled down to room temperature and finally the spectra were collected (Fig. 9A, spectra b).

Methanol adsorbed on Cu/MgO after exposure for 5 min at 300 °C (under vacuum) resulted in the formation of dominant species with the bands at 1650 and 1475–1455 cm^{-1}. All these features can be attributed to vibration modes of monodentate and bidentate carbonate/bicarbonates (e.g. Köck et al., 2013). Simultaneously, the weak 1650 cm^{-1} band can be also attributed to water molecules formed as a product of methanol incineration and adsorbed on the catalyst surface. Carbon monoxide, another product of methanol oxidation, can be detected both in the gas phase (vibrational-rotational spectrum) and in forms of Cu(I)-carbonyls or Cu(0)-carbonyls, recognized as the bands at 2169 and 2132 cm^{-1}, Fig. 9B). The amount of carbon dioxide (the 2343 cm^{-1} band) was found to be negligible. Thus, it could be concluded that basic character of MgO results in a capture of CO_2 and its deposition in form of carbonates. It may be one of the possible factors influencing low catalytic activity of the Cu/MgO sample. It seems possible that carbonates deposited on the catalyst surface limit availability of copper species for methanol molecules.

For the Cu(5)–Mg–Al samples the amount of carbonates deposited on the catalyst surface was significantly lower (see the bands located at 1650 and 1475 cm^{-1}), while amount of CO_2 (the 2343 cm^{-1} band) was much higher in comparison to Cu/MgO. It is related to lower basicity of Cu(5)–Mg–Al than Cu/MgO and therefore, the lower affinity to CO_2 capture.

It should be noted that oxidation of adsorbed methanol occurred in the absence of gaseous oxygen and was induced by increase of temperature from RT to 300 °C. Thus, oxidation of methanol occurred by its reaction with surface oxygen ions of copper oxide species. Thus, it seems that one of the possible pathways of methanol conversion proceeds through adsorption of CH_3OH molecules and its oxidation by surface oxygen ions followed by reoxidation of copper species by gaseous oxygen. This hypothesis is also supported by H_2-TPR studies, which shows the correlation between red-ox properties of the catalysts and their activity in methanol incineration.

4. Conclusions

Synthesis, physicochemical characterization and activity in a total methanol oxidation of a series of the copper and/or manganese containing catalysts obtained from hydrotalcite-like materials were studied. It was shown that: (i) the copper containing hydrotalcite derived catalysts were much more active than calcined Mn-containing hydrotalcites; (ii) copper present in Mg–Al oxide matrix was found to be more catalytically active than copper impregnated on the Al_2O_3 and MgO supports; and (iii) doping of the hydrotalcite originated catalysts with a small amount of palladium promoter significantly improved their activity, especially in the low-temperature range. Moreover, it was suggested that one of the possible pathways of methanol conversion over the copper containing catalysts includes oxidation of chemisorbed CH_3OH molecules by

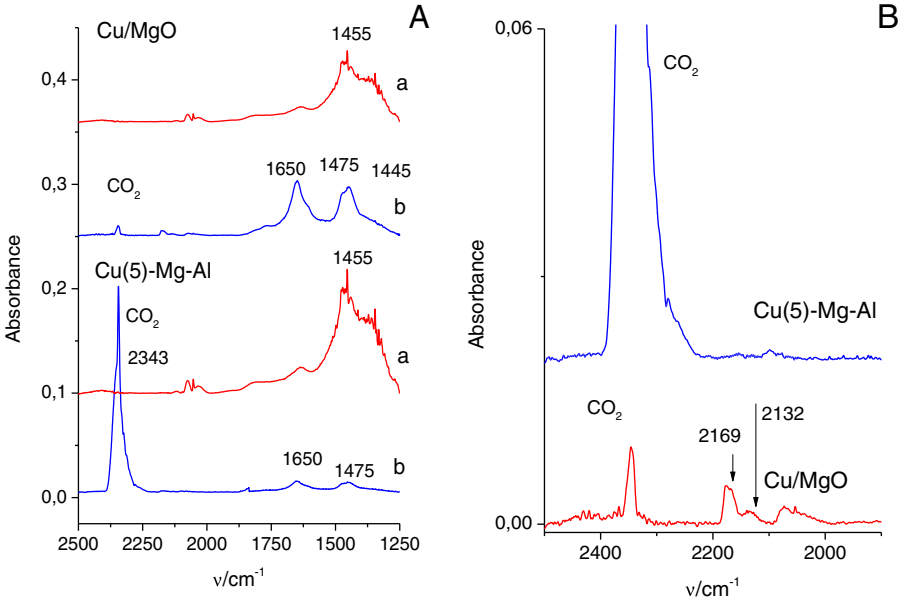

Fig. 9. (A) Infrared spectra collected for the studied catalysts after exposure of 1333 Pa methanol at RT (a) and spectra recorded at RT upon system heating to 300 °C for 5 min (b). (B) The region of C-O vibration in the spectra recorded at RT upon system heating to 300 °C for 5 min.

surface oxygen ions followed by reoxidation of copper species by gaseous oxygen.

Acknowledgments

The research was carried out with the equipment purchased thanks to the financial support of the European Regional Development Fund in the framework of the Polish Innovation Economy Operational Program (contract no. POIG.02.01.00-12-023/08).

References

Aguilera, D.A., Perez, A., Molina, R., Moreno, S., 2011. Cu–Mn and Co–Mn catalysts synthesized from hydrotalcites and their use in the oxidation of VOCs. Appl. Catal. B 104, 144–150.

Aramendía, M.A., Benítez, J.A., Borau, V., Jiménez, C., Marinas, J.M., Ruiz, J.R., Urbano, F., 1999. Study of MgO and Pt/MgO systems by XRD, TPR, and ^{1}H MAS NMR. Langmuir 15, 1192–1197.

Bahranowski, K., Bielańska, E., Janik, R., Machaj, T., Serwicka, E.M., 1999. LDH-derived catalysts for complete oxidation of volatile organic compounds. Clay Miner. 34, 67–77.

Baldi, M., Milella, F., Gallardo-Amores, J.M., Busca, G., 1998. A study of Mn-Ti oxide powders and their behaviour in propane oxidation catalysis. J. Mater. Chem. 8, 2525–2531.

Bastiani, R., Zonno, I.V., Santos, I.A.V., Henriques, C.A., Monteiro, J.E.L., Bastiani, R., Zonno, I.V., Santos, I.A.V., Henriques, C.A., Monteiro, J.E.L., 2004. Influence of thermal treatments on the basic and catalytic properties of Mg, Al-mixed oxides derived from hydrotalcites. Braz. J. Chem. Eng. 21, 193–202.

Brouet, G., Chen, X., Lee, C.W., Kevan, L., 1992. Evaluation of manganese (II) framework substitution in MnAPO-11 and Mn-impregnated AlPO4-11 molecular sieves by electron spin resonance and electron spin-echo modulation spectroscopy. J. Am. Chem. Soc. 114, 3720–3726.

Carnö, J., Ferrandon, M., Björnbom, E., Järås, S., 1997. Mixed manganese oxide/platinum catalysts for total oxidation of model gas from wood boilers. Appl. Catal. A 155, 265–281.

Centi, G., Perathoner, S., Biglino, D., Giamello, E., 1995. Adsorption and reactivity of NO on copper-on-alumina catalysts: I. Formation of nitrate species and their influence on reactivity in NO and NH_3 conversion. J. Catal. 151, 75–92.

Cheng, J., Yu, J., Wang, X., Li, L., Li, J., Hao, Z., 2008. Novel CH_4 combustion catalysts derived from Cu–Co/X-Al (X = Fe, Mn, La, Ce) hydrotalcite-like compounds. Energy Fuels 22, 2131–2137.

Chmielarz, L., Kuśtrowski, P., Rafalska-Łasocha, A., Dziembaj, R., 2003. Influence of Cu, Co and Ni cations incorporated in brucite-type layers on thermal behaviour of hydrotalcites and reducibility of the derived mixed oxide systems. Termochimica Acta 395, 225–236.

Chmielarz, L., Węgrzyn, A., Wojciechowska, M., Witkowski, S., Michalik, M., 2011. Selective catalytic oxidation (SCO) of ammonia to nitrogen over hydrotalcite originated Mg–Cu–Fe mixed metal oxides. Catal. Lett. 141, 1345–1354.

Chmielarz, L., Piwowarska, Z., Rutkowska, M., Wojciechowska, M., Dudek, B., Witkowski, S., Michalik, M., 2012. Total oxidation of selected mono-carbon VOCs over hydrotalcite originated metal oxide catalysts. Catal. Commun. 17, 118–125.

Cordi, E.M., Falconer, J.L., 1996. Oxidation of volatile organic compounds on Al_2O_3, Pd/Al_2O_3 and PdO/Al_2O_3 catalysts. J. Catal. 162, 104–117.

Crivello, M., Pérez, C., Herrero, E., Ghione, G., Casuscelli, S., Rodríguez-Castellón, E., 2005. Characterization of Al–Cu and Al–Cu–Mg mixed oxides and their catalytic activity in dehydrogenation of 2-octanol. Catal. Today 107–108, 215–222.

Dula, R., Janik, R., Machej, T., Stoch, J., Grabowski, R., Serwicka, E.M., 2007. Mn-containing catalytic materials for the total combustion of toluene: the role of Mn localisation in the structure of LDH precursor. Catal. Today 119, 327–331.

Gandia, L.M., Vicente, M.A., Gil, A., 2002. Complete oxidation of acetone over manganese oxide catalysts supported on alumina- and zirconia-pillared clays. Appl. Catal. B 38, 295–307.

Gaspar, A.B., Dieguez, L.C., 2000. Dispersion stability and methylcyclopentane hydrogenolysis in Pd/Al_2O_3 catalysts. Appl. Catal. A 201, 241–251.

Gauthard, F., Epron, F., Barbier, J., 2003. Palladium and platinum-based catalysts in the catalytic reduction of nitrate in water: effect of copper, silver, or gold addition. J. Catal. 220, 182–191.

Hassanzadeh, A., Abbasian, J., 2010. Regenerable MgO-based sorbents for high-temperature CO_2 removal from syngas: 1. Sorbent development, evaluation, and reaction modeling. Fuel 89, 1287–1297.

Hosseini, M., Siffert, S., Cousin, R., Aboukaïs, A., Hadj-Sadok, Z., Su, B.L., 2009. Total oxidation of VOCs on Pd and/or Au supported on TiO_2/ZrO_2 followed by "operanto" DRIFT. C. R. Chim. 12, 654–659.

Ivanova, A.S., Slavinskaya, E.M., Gulyaev, R.V., Zaikovskii, V.I., Stonkus, O.A., Danilova, I.G., Plyasova, L.M., Polukhina, I.A., Boronin, A.I., 2010. Metal–support interactions in Pt/Al_2O_3 and Pd/Al_2O_3 catalysts for CO oxidation. Appl. Catal. B 97, 57–71.

Jirátová, K., Čuba, P., Kovanda, F., Hilaire, L., Pitchon, V., 2002. Preparation and characterization of activated Ni (Mn)/Mg/Al hydrotalcites for combustion catalysis. Catal. Today 76, 43–56.

Kijlstra, W.S., Poels, E.K., Bliek, A., Weckhuysen, B.M., Schoonheydt, R.A., 1997. Characterization of Al_2O_3-supported manganese oxides by electron spin resonance and diffuse reflectance spectroscopy. J. Phys. Chem. B 101, 309–316.

Köck, E.M., Kogler, M., Bielz, T., Klötzer, B., Penner, S., 2013. In situ FT-IR spectroscopic study of CO_2 and CO adsorption on Y_2O_3, ZrO_2, and yttria-stabilized ZrO_2. J. Phys. Chem. C 117, 17666–17673.

Kosova, N.V., Asanov, I.P., Devyatkina, E.T., Avvakumov, E.G., 1999. State of manganese atoms during the mechanochemical synthesis of $LiMn_2O_4$. J. Solid State Chem. 146, 184–188.

Kovanda, F., Jirátová, K., 2011a. Supported mixed oxide catalysts for the total oxidation of volatile organic compounds. Catal. Today 176, 110–115.

Kovanda, F., Jirátová, K., 2011b. Supported layered double hydroxide-related mixed oxides and their application in the total oxidation of volatile organic compounds. Appl. Clay Sci. 53, 305–316.

Kovanda, F., Jirátová, K., Rymeš, J., Koloušek, D., 2001. Characterization of activated Cu/Mg/Al hydrotalcites and their catalytic activity in toluene combustion. Appl. Clay Sci. 18, 71–80.

Kovanda, F., Grygar, T., Dorničák, V., Rojka, T., Bezdičká, P., Jirátová, K., 2005. Thermal behaviour of Cu–Mg–Mn and Ni–Mg–Mn layered double hydroxides and characterization of formed oxides. Appl. Catal. B 28, 121–136.

Kovanda, F., Rojka, T., Dobešová, J., Machovič, V., Bezdička, P., Obalová, L., Jirátová, K., Grygar, T., 2006. Mixed oxides obtained from Co and Mn containing layered double hydroxides: preparation, characterization, and catalytic properties. J. Solid State Chem. 179, 812–823.

Lamonier, J.F., Boutoundou, A.B., Gennequin, C., Pérez-Zurita, M.J., Siffert, S., Aboukais, A., 2007. Catalytic removal of toluene in air over Co–Mn–Al nano-oxides synthesized by hydrotalcite route. Catal. Lett. 118, 165–172.

Levi, Z., Raitsimring, A.M., Goldfarb, D., 1991. ESR and electron spin-echo studies of MnAlPO5. J. Phys. Chem. 95, 7830–7838.

Li, X., Xu, J., Zhou, L., Wang, F., Gao, J., Chen, Ch., Ning, J., Ma, H., 2006. Liquid-phase oxidation of toluene by molecular oxygen over copper manganese oxides. Catal. Lett. 110, 149–154.

Ludvíková, J., Jirátová, K., Kovanda, F., 2012. Mixed oxides of transition metals as catalysts for total ethanol oxidation. Chem. Pap. 66, 589–597.

Marion, M.C., Grabowski, E., Primet, M., 1990. Physicochemical properties of copper oxide loaded alumina in methane combustion. J. Chem. Soc. Faraday Trans. 86, 3027–3032.

Mendes, F.M.T., Schmal, M., 1997. The cyclohexanol dehydrogenation on Rh-Cu/Al_2O_3 catalysts Part 1. Characterization of the catalyst. Appl. Catal. A 151, 393–408.

Mikulová, Z., Čuba, P., Balabánová, J., Rojka, T., Kovanda, F., Jirátová, K., 2007. Calcined Ni–Al layered double hydroxide as a catalysts for total oxidation of volatile organic compounds: effect of precursor crystallinity. Chem. Pap. 61, 103–109.

Millange, F., Walton, R.I., O'Hare, D., 2000. Time-resolved *in situ* X-ray diffraction of the liquid-phase reconstruction of Mg–Al-carbonate hydrotalcite-like compounds. J. Mater. Chem. 10, 1713–1720.

Okumura, K., Kobayashi, T., Tanaka, H., Niwa, M., 2003. Toluene combustion over palladium supported on various metal oxide supports. Appl. Catal. B 44, 325–331.

Palacio, L.A., Velásquez, J., Echavarría, A., Faro, A., 2010. Total oxidation of toluene over calcined trimetallic hydrotalcites type catalysts. J. Hazard. Mater. 177, 407–413.

Stobbe, E.R., de Boer, B.A., Geus, J.W., 1999. The reduction and oxidation behaviour of manganese oxides. Catal. Today 47, 161–167.

Tang, X., Li, J., Sun, L., Hao, J., 2010. Origination of N_2O from NO reduction by NH_3 over β-MnO_2 and α-Mn_2O_3. Appl. Catal. B 99, 156–162.

Velu, S., Shah, N., Jyothi, T.M., Sivasanker, S., 1999. Effect of manganese substitution on the physicochemical properties and catalytic toluene oxidation activities of Mg–Al layered double hydroxides. Microporous Mesoporous Mater. 33, 61–75.

Węgrzyn, A., Rafalska-Łasocha, A., Majda, D., Dziembaj, R., Papp, H., 2010. The influence of mixed anionic composition of Mg–Al hydrotalcites on the thermal decomposition mechanism based on in situ study. J. Therm. Anal. Calorim. 99, 443–457.

Xu, J., Luan, X.Z., Wasowicz, T., Kevan, L., 1998. ESR and ESEM studies of Mn-containing MCM-41 materials. Microporous Mesoporous Mater. 22, 179–191.

Zimowska, M., Michalik-Zym, A., Janik, R., Machej, T., Gurgul, J., Socha, R.P., Podobiński, J., Serwicka, E.M., 2007. Catalytic combustion of toluene over Cu–Mn oxides. Catal. Today 119, 321–326.